Tuning Aromaticity in Trigonal Alkaline Earth Metal Clusters and Their Alkali Metal Salts

J. OSCAR C. JIMÉNEZ-HALLA,[1] EDUARD MATITO,[2] LLUÍS BLANCAFORT,[1] JUVENCIO ROBLES,[3] MIQUEL SOLÀ[1]

[1]*Institut de Química Computacional and Departament de Química, Universitat de Girona, Campus de Montilivi, 17071 Girona, Catalonia, Spain*

[2]*Department of Chemistry, The Lundbeck Foundation Center for Theoretical Chemistry, University of Aarhus, Langelandsgade 140, DK-8000 Aarhus C, Denmark*

[3]*Departamento de Farmacia, División de Ciencias Naturales y Exactas, Universidad de Guanajuato, Noria Alta s/n 36050 Guanajuato, Gto. Mexico*

Received 19 December 2008; Revised 5 March 2009; Accepted 9 March 2009

DOI 10.1002/jcc.21291

Published online 30 April 2009 in Wiley InterScience (www.interscience.wiley.com).

Abstract: In this work, we analyze the geometry and electronic structure of the $[X_nM_3]^{n-2}$ species (M = Be, Mg, and Ca; X = Li, Na, and K; n = 0, 1, and 2), with special emphasis on the electron delocalization properties and aromaticity of the *cyclo*-$[M_3]^{2-}$ unit. The *cyclo*-$[M_3]^{2-}$ ring is held together through a three-center two-electron bond of σ-character. Interestingly, the interaction of these small clusters with alkali metals stabilizes the *cyclo*-$[M_3]^{2-}$ ring and leads to a change from σ-aromaticity in the bound state of the *cyclo*-$[M_3]^{2-}$ to π-aromaticity in the XM_3^- and X_2M_3 metallic clusters. Our results also show that the aromaticity of the *cyclo*-$[M_3]^{2-}$ unit in the X_2M_3 metallic clusters depends on the nature of X and M. Moreover, we explored the possibility for tuning the aromaticity by simply moving X perpendicularly to the center of the M_3 ring. The Na_2Mg_3, Li_2Mg_3, and X_2Ca_3 clusters undergo drastic aromaticity alterations when changing the distance from X to the center of the M_3 ring, whereas X_2Be_3 and K_2Mg_3 keep its aromaticity relatively constant along this process.

 J Comput Chem 30: 2764–2776, 2009

Key words: 3c-2e bonding; alkaline earth metal clusters; σ-aromaticity; π-aromaticity; aromaticity tuning; DFT calculations

Introduction

All-metal aromatic clusters represent one of the most exciting species synthesized in the beginning of this 21st century.[1] These species have attracted the attention of both basic and applied researchers as they are worth studying, on one side, for their differential physicochemical properties and, on the other, for their potential application in the field of nanomaterials.[2–5] These all-metal clusters present several common features with organic aromatic compounds, such as stabilization upon complexation to transition metals (through $Fe(CO)_3$ complexes[3] or by metal sandwich complexes[6,7]), substitution reactions with conventional organometallic complexes,[3] or the formation of superclusters.[3,8] In contrast with its π-conjugated organic analogues, all-metal clusters possess exalted linear and nonlinear optical properties such as higher polarizability or higher second hyperpolarizability.[9] In addition, while classical conjugated organic compounds possess only π-(anti)aromaticity (with some relevant exceptions having double π- and σ-aromaticity like the D_{3h} 3,5-dehydrophenyl cation[10] among others[11]), all-metal clusters and inorganic compounds can have not only the conventional π-(anti)aromaticity, but also σ-[12,13] or even δ-[14] and φ-(anti)aromaticity,[15] thus giving rise to the so-called multifold aromaticity.[2,16]

Among all-metal aromatic species, the simplest metal cluster exhibiting aromatic character is the *cyclo*-$[Li_3]^+$.[4,12,17] This species shows σ-aromaticity with a completely delocalized electron pair in a nonclassical three-center two-electron (3c-2e) bond, similar to that found for the conventional σ-aromatic H_3^+[17,18]

Additional Supporting Information may be found in the online version of this article.

Correspondence to: E. Matito; e-mail: ematito@gmail.com; or M. Solà; e-mail: miquel.sola@udg.edu

Contract/grant sponsor: Spanish MEC; contract/grant number: CTQ2008-03077/BQU

Contract/grant sponsor: Catalan Departament d'Universitats, Recerca i Societat de la Informació (DURSI); contract/grant number: 2005SGR-00238

Contract/grant sponsor: Generalitat de Catalunya and Social European Fund; contract/grant number: 2005FI/00451

and cyclopropane species,[19] among others.[20] For this species, the electron density delocalized in the center of three-membered rings leads to specific magnetic properties.[21] Let us mention here that the aromaticity of *cyclo*-$[Li_3]^+$ is, however, somewhat more controversial than that of H_3^+, as the Li_3^+ in contrast to H_3^+ does not show the characteristic diatropic ring-current of aromatic species.[17]

Kuznetsov and Boldyrev (KB)[22] have studied the $NaMg_3^-$ and Na_2Mg_3 bimetallic clusters having the unusual *cyclo*-$[Mg_3]^{2-}$ trigonal planar cluster as the basic structural unit. According to the electronic structure and NICS(0) calculations by KB, the *cyclo*-$[Mg_3]^{2-}$ unit in $NaMg_3^-$ and Na_2Mg_3 has a pair of π-delocalized electrons which gives π-aromatic character to the cluster without the formation of a σ-framework. During the course of a recent study,[23] we found through the inspection of the shape of occupied molecular orbitals (MOs) that the isolated *cyclo*-$[Mg_3]^{2-}$ cluster has exclusively σ-aromaticity like the analogous *cyclo*-$[Li_3]^+$.[4,12,17] Apparently, it is the interaction with the Na^+ that triggers off a shift from σ-aromaticity in *cyclo*-$[Mg_3]^{2-}$ to π-aromaticity in the $NaMg_3^-$ and Na_2Mg_3 metallic clusters. More recently, Roy and Chattaraj[24] (RC) have analyzed the aromaticity of D_{3h} *cyclo*-$[Be_3]^{2-}$ and of its complexes XBe_3^- and X_2Be_3 (X = Li, Na, and Cu). The authors found that the *cyclo*-$[Be_3]^{2-}$ unit is highly π-aromatic in nature according to nucleus-independent chemical shift (NICS),[25–27] polarizability, hardness, and electrophilicity values. The aromatic *cyclo*-$[Be_3]^{2-}$ and *cyclo*-$[Mg_3]^{2-}$ units have also been studied by Chattaraj and Giri (CG), who discussed their stabilization through the formation of sandwich-like complexes.[7]

Inspired by the change from σ-aromaticity in free *cyclo*-$[Mg_3]^{2-}$ to π-aromaticity in the alkali metal complexed salts, we decided to undertake a detailed investigation of the trigonal alkaline earth metal clusters and their alkaline salts, i.e., the $[X_nM_3]^{n-2}$ species (M = Be, Mg, and Ca; X = Li, Na, and K; n = 0, 1, and 2) with a threefold purpose: first, to obtain a set of consistent structural data for the $[X_nM_3]^{n-2}$ species; second, to analyze the electronic structure, electron delocalization properties, and aromaticity of these species; and finally, to discuss aromaticity changes as a function of the distance from the alkali metal to the center of the M_3 ring.

Computational Details

All geometry optimizations were performed with the B3LYP functional[28] using the 6-311+G(d) basis set[29] by means of the Gaussian03 package of programs.[30] Vibrational frequencies were computed to verify the nature of the optimized minima. To obtain two-center electron sharing indexes (2c-ESI)[31] and the three-center counterparts (3c-ESI),[32,33] the ESI-3D software[34] was used. Within the formalism of the so-called Generalized Population Analysis (GPA),[33,35,36] different partitions of N electrons [eq. (1)] can be reached for each value of k (i.e., for $k = 2$, Δ_{AB} gives 2c-ESI and for $k = 3$, Δ_{ABC} corresponds to 3c-ESI) as follows:

$$N = \sum_A \Delta_A^{(k)} + \sum_{A<B} \Delta_{AB}^{(k)} + \sum_{A<B<C} \Delta_{ABC}^{(k)} + \ldots \sum_{A<B<C\ldots<K} \Delta_{ABC\ldots K}^{(k)} \quad (1)$$

where $A,B,C\ldots$K are the atoms involved and Δ_A contains the monoatomic terms, Δ_{AB} diatomic terms and so on. The way in which an atom in a molecule is defined (the partition used) gives rise to different ESIs. For instance, we may define a partition in the 3D space following an Atoms-in-Molecules (QTAIM) scheme or either we can distribute our basis functions in different atomic centers as it is done in a Mulliken-like approach. In our study, we have found that QTAIM defines nonnuclear attractor (NNA) regions that cannot be directly associated to a given atomic region. In this work, we address the dissociation of some species for which the use of diffuse functions is mandatory for an accurate description of the process. Since diffuse functions cannot be straightforwardly assigned to a given center, the use of Mulliken partition in this context is not recommended. In that event, one may consider the use of fuzzy-atom partition, which employs empirical radii to construct weight functions for each atom in the molecule.[37] As shown by some of us,[38] the dissociation of species bonded by a closed-shell interaction into neutral fragments, needs to use an atomic partition that can change along the dissociation process. Therefore, fuzzy-atom partition is not the candidate of choice in this context. An alternative to fuzzy-atom approach is the Becke-rho method,[38] which avoids the arbitrary use of radii by employing partial information of the electron density to replace the atomic radii. Namely, the weight functions of a given pair of atoms cross in the point with minimal density along the line between the two centers. Notice that in some cases this point coincides with the bond critical point (BCP) defined in QTAIM and it is then natural that this approach gives numbers close to QTAIM. However, the approach has the advantage of not presenting NNAs, and it was used successfully to describe dissociation reactions similar to the ones presented in this study.[38] Thus, we have adopted this partition in the present work.

The performance of the integration was checked by assessing that the sum of electron populations equals the number of electrons in the molecule. Such criterion was fulfilled with precision up to 0.001 electrons. Calculation of these 2c-ESI and 3c-ESI within the density functional theory (DFT) cannot be performed exactly because pair density (or higher-order densities) are not available at this level of theory.[39] As an approximation, we have used the Kohn-Sham orbitals obtained from a B3LYP/6-311+G(d) calculation to compute Hartree-Fock-like ESIs. In practice, the values of the ESIs obtained using this approximation are generally closer to the Hartree-Fock values than correlated ESIs obtained with a configuration interaction method.[38,39] The atomic overlap matrices needed for the calculation of 2c- and 3c-ESIs were computed with the FUZZY program.[40]

In a recent work, we showed that NICS profiles can be used to characterize aromaticity in inorganic species and to classify inorganic clusters into aromatic, nonaromatic, and antiaromatic categories.[23] More recently, Stanger[41] has checked the performance of this method for organic species and Tsipis et al.[42] have applied it to study *cyclo*-Cu_3Au_3 homotops. In this work, we use NICS profiles to classify the studied compounds and to analyze the $[X_2M_3]$ regions where the changes in aromaticity as a function of the distance from the alkali metal to the center of the Mg_3 ring are more important. Although several authors have emphasized the need of using various aromaticity descriptors to correctly assess the aromatic character in a given species,[4,26,43]

other aromaticity descriptors such as PDI,[44] FLU,[45] HOMA,[46] or ASE[47] are not straightforwardly applicable in this context. In the case of PDI, the reason is that this descriptor can be employed only in six-membered rings. FLU and HOMA cannot be used here because of the necessity of a reference system that has not been defined yet for the present systems. Finally, for ASE the problem is to find homodesmotic schemes that have the same number of bonds between the given atoms in each state of hybridization both in products and reactants. In addition, the necessary corrections for conjugation, hyperconjugation, and protobranching[48] to produce correct ASE values are still unknown in the field of inorganic compounds. Therefore, we have restricted our aromaticity study to both 3c-ESI and NICS indices. Different studies have shown that multicenter ESIs are good descriptors of aromaticity in organic species,[36,49,50] whereas NICS is probably the most widely used index of aromaticity.

The GIAO method[51] has been used to perform calculations of NICS at ring centers (NICS(0)) determined by the nonweighted mean of the heavy atoms coordinates and at 1 Å above or below the center of the ring (NICS(1)). We have also analyzed the out-of-plane components of the NICS(0) and NICS(1), which are $NICS(0)_{zz}$ and $NICS(1)_{zz}$, respectively. The latter measure is, according to Schleyer et al.,[52] one of the most reliable indicators of aromaticity among the existing NICS measures together with $NICS(0)_{zz,\pi}$. Moreover, in selected cases, we have decomposed the NICS indices into their molecular orbital components[27,52] using the NBO 5.0 program.[53]

Finally, we have used the electron localization function (ELF)[54] to get more insight about the nature of the chemical bond between the Na cation and the $[Mg_3]^{2-}$ unit in $NaMg_3^-$. The ELF has been extensively used in the literature to analyze the chemical bonding in molecular species,[55] to distinguish between different reaction mechanisms[56] or to account for the aromaticity of molecular systems.[57] In this work, we have used the TopMod package[58] to perform the analysis.

Results and Discussion

In Figure 1, we present the geometries of the ground state of *cyclo*-$[Mg_3]^{2-}$ (D_{3h}, $^1A_1'$), $NaMg_3^-$ (C_{3v}, $^1A_1$), and Na_2Mg_3 (D_{3h}, $^1A_1'$) species. To check whether we got the correct electronic state of *cyclo*-$[Mg_3]^{2-}$, we have calculated the energy of two possible low-lying closed-shell singlet electronic states, namely, the $^1A_1'(\sigma)$ electronic state of *cyclo*-$[Mg_3]^{2-}$ with two electrons occupying the HOMO of σ-symmetry and the $^1A_1'(\pi)$ electronic state with the two σ-electrons of the initial HOMO promoted to the LUMO of π-symmetry (Fig. 2a). The latter was considered by CG[7] as the ground state of *cyclo*-$[Mg_3]^{2-}$. B3LYP/6-311+G(d) calculations show that the $^1A_1'(\sigma)$ electronic state of *cyclo*-$[Mg_3]^{2-}$ is 5.3 kcal mol^{-1} lower in energy than the $^1A_1'(\pi)$ electronic state. More refined CCSD(T)/6-311+G(d) and CASPT2//CASSCF(8,9)/6-311+G* results in which the geometry optimization of the two states was taken into account further confirm this trend by giving the $^1A_1'(\sigma)$ electronic state more stable than the $^1A_1'(\pi)$ by 3.6 and 5.0 kcal mol^{-1}, respectively. We have also checked that the $^1A_1'(\sigma)$ ground electronic state is more stable than the open-shell singlet $^1A_2''$ and triplet $^3A_2''$ states. CASPT2//CASSCF(8,9)/6-311+G* results indicate that the open-shell singlet $^1A_2''$ is 2.7 kcal mol^{-1} lower in energy than the $^1A_1'(\pi)$ state, and therefore, the $^1A_2''$ state must be considered the lowest-lying singlet *excited* state. In our opinion, these calculations unambiguously establish that the $^1A_1'(\sigma)$ (and not the $^1A_1'(\pi)$) state is the *ground* state of the *cyclo*-$[Mg_3]^{2-}$ species.

Analogous calculations on *cyclo*-$[Mg_3]^-$ ($^2A_2''$, D_{3h}) determined that this molecule is more stable than the former one. Therefore, the *cyclo*-$[Mg_3]^{2-}$ species is unstable with respect to the loss of an electron. It is important to note that *cyclo*-$[Mg_3]^-$ species has been detected in photoelectron spectra experiments.[59] Because of the instability of the *cyclo*-$[Mg_3]^{2-}$ species, the only way to study this dianionic cluster experimentally is through electron scattering experiments. Depending on the size of the repulsive Coulomb barrier for electron detachment found by the excess electron in *cyclo*-$[Mg_3]^{2-}$ species, this isolated dianion can have a bound state with a substantial or short lifetime. If the isolated metastable dianion is relatively stable, then the addition of moderately diffuse functions should not change significantly the results obtained for the different molecular properties. In a recent important work, Lambrecht et al.[60] have shown that the properties of Al_4^{2-}, which is also unstable when compared with Al_4^- + free e^-, change significantly when increasing the number of diffuse functions in the basis set. After inclusion of certain number of diffuse functions, the Al_4^{2-} evolves to Al_4^- + free e^-. In this sense, Lambrecht et al.[60] warned about the validity of calculations carried out for unstable dianions. The problem is that the molecular properties change from those of the bound state of Al_4^{2-} to those of Al_4^- + free e^- by adding more and more diffuse functions. In a recent comment[61] (see also the rebuttal in ref. 62) on the work by Lambrecht et al.,[60] Zubarev and Boldyrev argued against this point of view by saying that "the bound state of individual Al_4^{2-} is an adequate model of Al_4^{2-} in stabilizing environment such as in $NaAl_4^-$ or Na_2Al_4 (...) when Al_4^{2-} is stabilized by the external field, the 'tails' of continuum solutions can be disregarded". They also considered that calculations for isolated Al_4^{2-} species using a 6-311+G(d) basis provide an adequate model for the Al_4^{2-} unit embedded in a stabilizing environment. Following the Zubarev and Boldyrev arguments,[61] we will assess the properties of the bound state in a metastable dianion, such as *cyclo*-$[Mg_3]^{2-}$ by employing the 6-311+G(d) basis set.

The unstable *cyclo*-$[Mg_3]^{2-}$ ring can be stabilized by interaction with alkali metal cations, such as Na^+, yielding the $[Na_nMg_3]^{n-2}$ species (n = 1 and 2) that contain a Mg_3 unit whose properties may resemble those of the bound state of *cyclo*-$[Mg_3]^{2-}$. In this work, we focus our interest, first, in the $NaMg_3^-$ and Na_2Mg_3 bimetallic clusters already discussed by KB in a previous work.[22] Second, we analyze the effect of changing the nature of the alkali metal cation in the $[X_nMg_3]^{n-2}$ species (X = Li and K; n = 1 and 2). Third, we discuss the molecular and electronic structure of the $[X_nM_3]^{n-2}$ species (M = Be and Ca, X = Li, Na, and K; n = 0, 1, and 2). And finally, for the $[X_2M_3]$ (M = Be, Mg, and Ca, X = Li, Na, and K) compounds, we examine the effect of increasing the distance from X to the center of the M_3 unit on the aromaticity of the

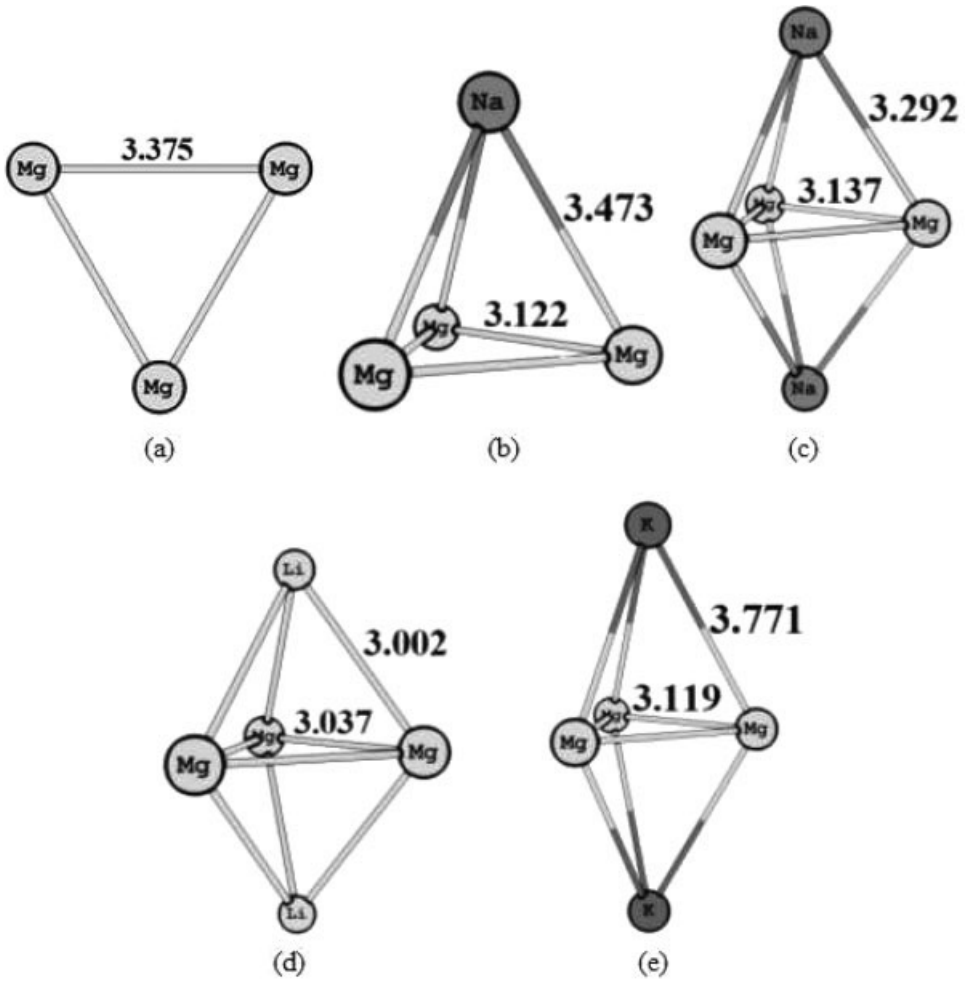

Figure 1. B3LYP/6-311+G(d) optimized structures for (a) trigonal planar *cyclo*-$[Mg_3]^{2-}$ (D_{3h}, $^1A_1'$), (b) trigonal pyramidal $NaMg_3^-$ (C_{3v}, $^1A_1$), (c) bipyramidal Na_2Mg_3 (D_{3h}, $^1A_1'$), (d) bipyramidal Li_2Mg_3 (D_{3h}, $^1A_1'$), and (e) bipyramidal K_2Mg_3 (D_{3h}, $^1A_1'$). Bond lengths are given in Å.

M_3 ring. Let us first begin with the analysis of the Na_2Mg_3 and $NaMg_3^-$ species.

Electronic Molecular Structure and Aromaticity of Cyclo-$[Mg_3]^{2-}$, $NaMg_3^-$, and Na_2Mg_3

The molecular orbitals (MOs) of valence electrons obtained for $NaMg_3^-$, Na_2Mg_3, and *cyclo*-$[Mg_3]^{2-}$ have been depicted in Figure 2. One can observe that the three species share almost the same set of MOs. The main difference corresponds to the frontier MOs that are exchanged. Thus, the HOMO in *cyclo*-$[Mg_3]^{2-}$ becomes the LUMO in the $NaMg_3^-$ and Na_2Mg_3 bimetallic clusters and vice versa. As a consequence, the 3c-2e bond becomes of π-character in $NaMg_3^-$ and Na_2Mg_3 as pointed out by KB.[22] The reason for this change is the fact that the pair of electrons responsible for the 3c-2e bond interacts better with the Na^+ cations in the π- than in the σ-MO both from an electrostatic and covalent (better $HOMO_{Mg3} - LUMO_{Na}$ overlaps) points of view.

Table 1. Total and π Two-Center (2c), Mg—Mg, and Three-Center (3c), Mg—Mg—Mg, Electron Sharing Indices (ESI, in Electrons), and NICS (in ppm) Indices for *cyclo*-$[Mg_3]^{2-}$ (D_{3h}, $^1A_1'$), $NaMg_3^-$ (C_{3v}, $^1A_1$), and Na_2Mg_3 (D_{3h}, $^1A_1'$) Calculated at B3LYP/6-311+G(d) Level of Theory.

Index	Mg_3^{2-}	$NaMg_3^-$	Na_2Mg_3
2c-ESI	1.303	1.092	0.947
2c-ESI π	0.000	0.172	0.190
3c-ESI	0.458	0.306	0.255
3c-ESI π	0.000	0.070	0.066
NICS(0)	−2.85	−22.58	−28.86
$NICS(0)_{ZZ}$	−12.72	−17.92	−21.38
NICS(1)	−4.00	−20.69[a] (−15.33)[b]	−24.07
$NICS(1)_{ZZ}$	−12.21	−21.46[a] (−17.90)[b]	−24.82

[a]Measured in the direction to the cation.
[b]Measured in the opposite direction to the cation.

Table 2. Value of the ELF at the Attractors of the Basins, ELF, Population of the Basins, $N(\Omega_1)$, the Variance of the Population, $\sigma[N(\Omega_1)]^2$, and the Fluctuation Value, $\lambda_F(\Omega_1)$ for Mg_3Na^- Calculated at B3LYP/6-311+G(d) Level of Theory.

	Ω_1	ELF	$N(\Omega_1)$	$\sigma[N(\Omega_1)]^2$	$\lambda_F(\Omega_1)$	Contribution analysis (higher than 2%)
1	C(Mg1)	1.000	10.02	0.28	0.03	5 (85.2) 6 (7.4) 7 (7.4)
2	C(Mg2)	1.000	10.02	0.28	0.03	5 (7.4) 6 (7.4) 7 (85.2)
3	C(Mg3)	1.000	10.02	0.28	0.03	5 (7.4) 6 (85.2) 7 (7.4)
4	C(Na)	1.000	10.04	0.2	0.02	5 (21.1) 6 (21.1) 7 (21.1) 8 (36.8)
5	V(Mg1,Na)	0.960	2.41	1.16	0.48	1 (20.7) 4 (3.6) 6 (30.6) 7 (30.6) 8 (10.8)
6	V(Mg3,Na)	0.960	2.41	1.16	0.48	3 (20.7) 4 (3.6) 5 (30.6) 7 (30.6) 8 (10.8)
7	V(Mg2,Na)	0.960	2.41	1.16	0.48	2 (20.7) 4 (3.6) 5 (30.6) 6 (30.6) 8 (10.8)
8	V(Na)	0.639	0.65	0.47	0.72	4 (16.3) 5 (27.9) 6 (27.9) 7 (27.9)

This exchange in the frontier MOs has remarkable effects. First, the Mg—Mg bond distance decreases from *cyclo*-$[Mg_3]^{2-}$ (3.37 Å) to $NaMg_3^-$ (3.12 Å) and Na_2Mg_3 (3.14 Å). Interestingly, the Mg—Mg bond distance in *cyclo*-$[Mg_3]^-$ is 3.16 Å and its electronic structure is similar to that of the $NaMg_3^-$ and Na_2Mg_3 species in Figure 2, the HOMO being a π-orbital and the LUMO a σ-orbital. Since when going from *cyclo*-$[Mg_3]^{2-}$ to $NaMg_3^-$, there is a partial charge transfer from $[Mg_3]^{2-}$ to Na^+, one may already expect that the Mg—Mg bond distances could be similar in *cyclo*-$[Mg_3]^-$ and $NaMg_3^-$. What is probably less expected is the reduction of the Mg—Mg bond distance when going from *cyclo*-$[Mg_3]^{2-}$ to $NaMg_3^-$ as it is usually said that σ- are stronger than π-interactions. However, in this particular case, the overlaps between Mg *3p* atomic orbitals (AOs) in the σ-HOMO of *cyclo*-$[Mg_3]^{2-}$, with *p*-orbitals pointing toward the center of the ring, are not necessarily larger than those between Mg *3p* AOs that give rise to the π-LUMO. In addition, the reduction of the Mg—Mg bond length favors the interaction of the Na^+ with the $[Mg_3]^{2-}$ unit. Second, when comparing the sequence: from *cyclo*-$[Mg_3]^{2-}$ to $NaMg_3^-$ and from this to Na_2Mg_3, a substantial reduction of the three-center ESI (3c-ESI) between Mg atoms is observed, in spite of the fact that there is still a positive and relative large value consistent with a 3c-2e bond[33] (Table 1). Such 3c-2e bond has a contribution of 23% (for $NaMg_3^-$) and 26% (for Na_2Mg_3) from π-orbitals (only contributions from the HOMO orbital in $NaMg_3^-$ and Na_2Mg_3 are considered in the evaluation of the π-character* of the 2c- and 3c-ESI[63]) in contrast with *cyclo*-$[Mg_3]^{2-}$ for which the 3c-ESI has exclusively σ-character. Third, the 2c-ESI in c*yclo*-$[Mg_3]^{2-}$ is also relatively high as expected from the covalent nature of the Mg—Mg bond; it has only σ-component and it is mainly due to the pair of electrons in the σ-HOMO orbital. When one or two Na^+ cations are coordinated in the center of the ring, we find a reduction of the Mg—Mg 2c-ESI, which acquires certain π-character (16–20%), due to the fact that some electrons are now delocalized between the Na and Mg atoms. Indeed, for Na_2Mg_3, the electron pair in the HOMO orbital is about 66% delocalized between Na and Mg atoms and only about 34% between Mg atoms.

To discuss the bonding mechanism of Na^+ with the $[Mg_3]^{2-}$ unit, we have analyzed the $NaMg_3^-$ system by means of the ELF. In Table 2, we have collected the data concerning this analysis and Figure 3 shows the ELF topology. The analysis reveals three bonding basins between Na and Mg, V(Mg,Na) with population of 2.41 e, highly delocalized (high variance and fluctuation values). In spite of being located closer to Mg atoms, these basins are significantly delocalized (14.4%) over the Na fragment (C(Na) and V(Na)); the remaining delocalization is mainly due to other V(Mg,Na) basins (61.2%) and the closer Mg core basins (20.7%). The valence basin associated to Na atom, V(Na) is located above the core basin, C(Na), farther from the $[Mg_3]$ unit. This basin, which contains 0.65 e, is also quite delocalized, particularly due to V(Mg,Na) basins (83.7%). Thus, there is an evident interaction between Mg and Na atoms. Although there is no trisynaptic basin in this system associated to three Mg atoms, the high delocalization between V(Mg,Na) neighboring basins, and the high value (ELF = 0.72) at which these three bonding basins are separated into individual localization domains (Fig. 3, l.h.s. above picture) indicates a certain degree of three-center bonding.

In their previous work, KB[22] confirmed the van der Waals nature of the bonding in the neutral trigonal planar *cyclo*-$[Mg_3]$ cluster.[64] KB also found that the unpaired electron in *cyclo*-$[Mg_3]^-$ occupies a delocalized π-MO that is responsible for the chemical bonding in this anionic cluster. For the bound state of isolated *cyclo*-$[Mg_3]^{2-}$, the bonding situation is completely different. As can be seen in Figure 2, the chemical bond in this species is due to the σ-electron pair that occupies the HOMO forming a 3c-2e bond similar to that of *cyclo*-$[Li_3]^+$. The presence of this 3c-2e bond is further substantiated by the positive and relatively large values of the 3c-ESI.[33] Because of the delocalized nature of the pair of electrons in the 3c-2e bond, the *cyclo*-$[Mg_3]^{2-}$ has σ-aromaticity. Indeed, this is confirmed by the NICS profiles of Figure 4, which point out a dramatic change in aromaticity due to Na^+ coordination. The values of NICS become clearly more negative as we move from *cyclo*-$[Mg_3]^{2-}$ to $NaMg_3^-$ and from this to Na_2Mg_3 (Table 1). Thus, according to the NICS values, the aromaticity of the Mg_3 unit is

*Because of the loss of symmetry in $NaMg_3^-$, one should talk about pseudo-π instead of π-orbitals in this species. It is worth noting that in this compound the maximum overlap between σ and π occupied molecular orbitals is smaller than 10^{-5} a.u., and, consequently, the σ/π separation in this compound is almost exact.

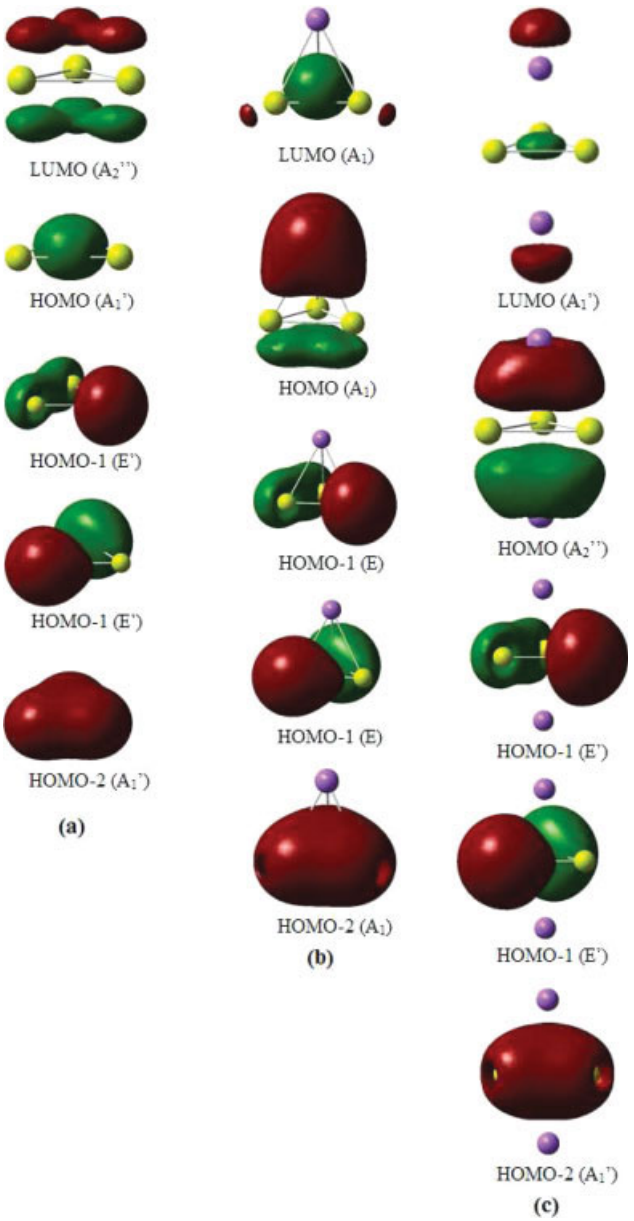

Figure 2. Valence molecular orbital plots for (a) *cyclo*-$[Mg_3]^{2-}$ (D_{3h}), (b) $NaMg_3^-$ (C_{3v}), and (c) Na_2Mg_3 (D_{3h}). Isosurfaces values are at 0.03 a.u. (We have checked the nature of these MOs by performing QCISD(T) and CASSCF(8,8) calculations with the same basis set. These calculations have provided identical shapes for the corresponding natural MOs).

larger in $NaMg_3^-$ and Na_2Mg_3 than in *cyclo*-$[Mg_3]^{2-}$. In contrast, the 3c-ESI values are clearly larger for isolated *cyclo*-$[Mg_3]^{2-}$ than in $NaMg_3^-$ and Na_2Mg_3, thus indicating a reduction of aromaticity of the $[Mg_3]$ unit due to the interaction with Na^+ cations.

For distances longer than *ca*. 2 Å from the center of the ring, the values of the NICS start to be influenced by the proximity of the Na^+ and for this reason this index calculated at such distances cannot be used to discuss aromaticity.[65] Obviously, for

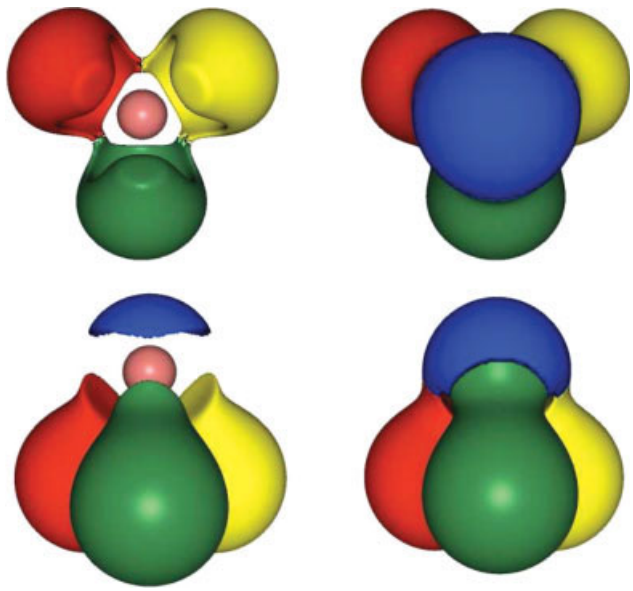

Figure 3. The ELF topology from different perspectives of Mg_3Na^- molecule (the pictures above with the C_3 axis perpendicular and the ones below with C_3 parallel to the molecular Mg_3 plane) and different isosurface values (ELF = 0.50 for the r.h.s pictures, and ELF = 0.70 above ELF = 0.60 below in the l.h.s.) In red, yellow and green the valence basins for Mg and Na, V(Mg, Na), in salmon the Na core basin, C(Na) and in blue the valence basin for Na, V(Na).

$NaMg_3^-$, we have two different NICS profiles as we move from the center of the ring in the same or in the opposite direction to the Na^+ cation, both depicted in Figure 4. It is worth noting that the *cyclo*-$[Mg_3]^{2-}$ and the $NaMg_3^-$ (down) NICS profiles coincide for values larger than 2.5 Å.

Finally, Table 3 gathers the most important molecular orbital contributions of the dissected NICS indices for *cyclo*-$[Mg_3]^{2-}$, $NaMg_3^-$, and Na_2Mg_3 species, and, in particular, of the large negative NICS(0) values. As can be seen, the largest contribution to the total NICS comes from the HOMO-2 orbital with the only exceptions of the NICS(1) of $NaMg_3^-$ and Na_2Mg_3 for which the contribution of the HOMO is the most important.

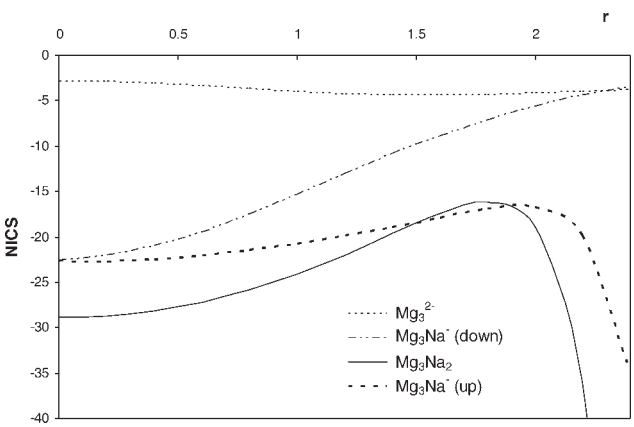

Figure 4. NICS profiles of the *cyclo*-$[Mg_3]^{2-}$, $NaMg_3^-$, and Na_2Mg_3 species.

Table 3. Values of the Dissected NICS (in ppm) Indices for the Highest Occupied Molecular Orbitals in *cyclo*-$[Mg_3]^{2-}$ (D_{3h}, $^1A_1'$), $NaMg_3^-$ (C_{3v}, $^1A_1$), and Na_2Mg_3 (D_{3h}, $^1A_1'$) Calculated at B3LYP/6-311+G(d) Level of Theory.

	Mg_3^{2-}			$NaMg_3$[a]			Na_2Mg_3		
Index	HOMO	HOMO-1[b]	HOMO-2	HOMO	HOMO-1[b]	HOMO-2	HOMO	HOMO-1[b]	HOMO-2
NICS(0)	−2.6	5.3	−10.9	−8.3	−1.4	−11.6	−8.8	−3.9	−12.0
$NICS(0)_{ZZ}$	−4.4	0.7	−12.4	−4.3	−1.9	−12.7	−4.8	−3.1	−12.5
NICS(1)	−3.0	2.7	−6.3	−6.2	−2.4	−4.5	−9.3	−3.3	−7.5
$NICS(1)_{ZZ}$	−3.4	0.0	−9.4	−5.1	−2.2	−9.0	−6.5	−3.0	−9.7

[a]Measured in the opposite direction to the cation.
[b]Doubly degenerated orbital.

Interestingly, the contribution of the HOMO-1 degenerated orbitals is in these three species relatively small. It is also worth noting that according to NICS the contribution to aromaticity is somewhat larger in the HOMO of π-symmetry of the $NaMg_3^-$ and Na_2Mg_3 species than in the HOMO of σ-symmetry of *cyclo*-$[Mg_3]^{2-}$.

The Effect of Changing the Nature of the Alkali Metals in the $[X_nMg_3]^{n-2}$ Species (X = Li and K; n = 1 and 2)

Table 4 contains the data of clusters of Mg_3^{2-} complexed by other alkali metals such as Li^+ or K^+, whereas Figure 1 depicts the molecular geometry of Li_2Mg_3 and K_2Mg_3 species (see also Figure S1 in Supporting Information for monocoordinated Mg_3^{2-} clusters). The changes in the molecular structure of the *cyclo*-$[Mg_3]^{2-}$ due to Li^+ or K^+ coordination are similar to those found in $NaMg_3^-$ and Na_2Mg_3, i.e., there is a small reduction of the Mg—Mg bond distance in the coordinated species. This reduction is particularly important (by more than 0.3 Å) for X = Li.

A reduction of 3c-ESI is observed when going from isolated *cyclo*-$[Mg_3]^{2-}$ to complexed $[X_nMg_3]^{n-2}$ species (X = Li and K; n = 1 and 2). Moreover, the π-component of the total 3c-ESI decreases from 95% ($LiMg_3^-$) to 21% (Li_2Mg_3) and from 60% (KMg_3^-) to 46% (K_2Mg_3). In general, this reduction of 3c-ESI goes with a reduction of 2c-ESI with the only exception of K_2Mg_3. According to the 3c-ESI values, the highest reduction of Mg—Mg—Mg electron delocalization with respect to Mg_3^{2-} cluster occurs for the Na_2Mg_3 system, followed by K_2Mg_3 > KMg_3^- > $NaMg_3^-$ > Li_2Mg_3 > $LiMg_3^-$. In general, the smallest differences in 2c- and 3c-ESIs between isolated and complexed *cyclo*-$[Mg_3]^{2-}$ species occur for X = Li. When the *cyclo*-$[M_3]^{2-}$ clusters are complexed with alkali metals, the effect in the 2c- and 3c-DIs depends on two opposing factors: first, the reduction of the M–M distances results in an increase of these 2c- and 3c-ESIs; second, the charge transfer from the *cyclo*-$[M_3]^{2-}$ clusters to the alkali metals reduces the electronic population of the ring and decreases the 2c- and 3c-ESIs between M atoms. We attribute the smaller changes in the 2c- and 3c-DIs induced by Li^+, when comparing with Na^+ and K^+, to the short Mg—Mg distance found in $LiMg_3^-$ and Li_2Mg_3.

The Electronic Molecular Structure and Aromaticity of $[X_nM_3]^{n-2}$ Species (M = Be and Ca, X = Li, Na, or K; n = 0, 1, and 2)

In this section, we analyze the effect of replacing Mg atoms by other alkaline earth metals such as Be or Ca. As found for the *cyclo*-$[Mg_3]^{2-}$ species in this study and for the *cyclo*-$[Be_3]^-$ reported by RC,[24] the *cyclo*-$[Be_3]^-$ and *cyclo*-$[Ca_3]^-$ are more stable than the *cyclo*-$[Be_3]^{2-}$ and *cyclo*-$[Ca_3]^{2-}$, respectively. However, these dianionic clusters become stable when complexed by alkali metals. The optimized geometries for these clusters are shown in Figures 5 and 6. See also Figures S2–S4 in Supporting Information where the corresponding molecular orbitals of these species are depicted. As we already discussed for the Mg clusters, M–M distances in the ring are shorter when the cations are incorporated. Interestingly, the interaction with Li^+ leads to the most compressed *cyclo*-$[M_3]^{2-}$ (M = Be, Mg, and Ca) units. It is important to remark here that the energy and geometry obtained by RC[24] for *cyclo*-$[Be_3]^{2-}$ and by CG[7] in *cyclo*-$[Mg_3]^{2-}$ differ from the present results despite RC and CG used the same method and basis set than us. We have checked that our results correspond to the ground state at the B3LYP/6-311+G(d) level (*vide supra*), whereas RC and GC reported one of the lowest-lying excited states of *cyclo*-$[Be_3]^{2-}$ and *cyclo*-$[Mg_3]^{2-}$ according to our calculations. On the other

Table 4. Total and π Two-Center (2c), Mg—Mg, and Three-Center (3c), Mg—Mg—Mg, Electron Sharing Indices (ESI, in Electrons), and NICS (in ppm) Indices for XMg_3^- (C_{3v}, $^1A_1$) and X_2Mg_3 (D_{3h}, $^1A_1'$), X = Li, K Calculated at B3LYP/6-311+G(d) Level of Theory.

Index	$LiMg_3^-$	KMg_3^-	Li_2Mg_3	K_2Mg_3
2c-ESI	1.226	0.864	1.157	0.964
2c-ESI π	0.289	0.235	0.283	0.193
3c-ESI	0.377	0.270	0.358	0.263
3c-ESI π	0.122	0.110	0.122	0.194
NICS(0)	−25.02	−21.53	−30.19	−27.64
$NICS(0)_{ZZ}$	−19.15	−18.03	−23.44	−22.08
NICS(1)	−22.24[a] (−17.39)[b]	−19.61[a] (−14.14)[b]	−24.09	−21.83
$NICS(1)_{ZZ}$	−21.91[a] (−19.23)[b]	−21.33[a] (−17.89)[b]	−25.72	−25.17

[a]Measured in the direction to the cation.
[b]Measured in the opposite direction to the cation.

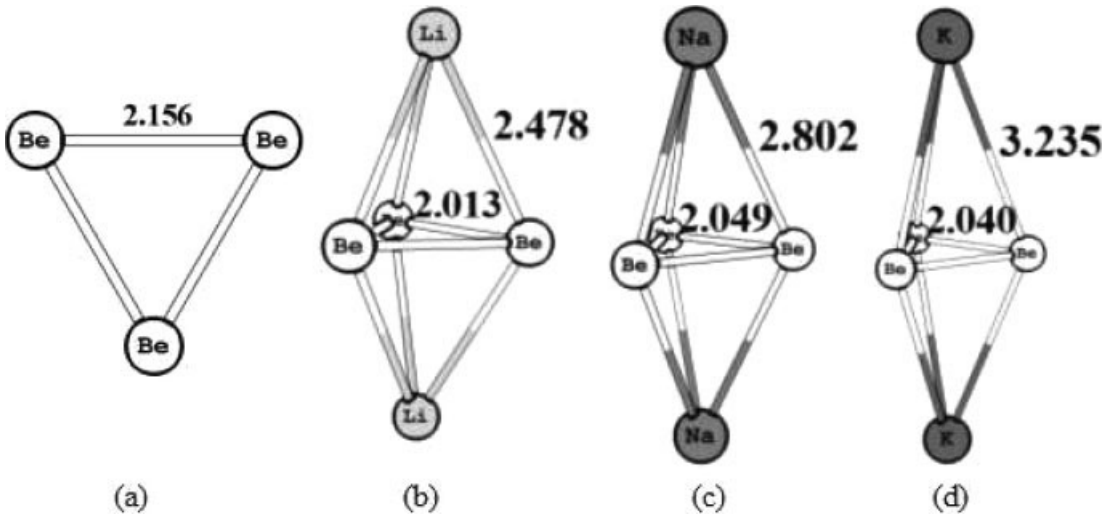

Figure 5. B3LYP/6-311+G(d) optimized structures of beryllium species for (a) trigonal planar *cyclo*-$[Be_3]^{2-}$ (D_{3h}, $^1A_1'$), (b) bipyramidal Li_2Be_3 (D_{3h}, $^1A_1'$), (c) bipyramidal Na_2Be_3 (D_{3h}, $^1A_1'$) and (d) bipyramidal K_2Be_3 (D_{3h}, $^1A_1'$). Bond lengths are given in Å.

hand, the RC[24] results for the $[X_nBe_3]^{n-2}$ species (X = Li, Na and n = 1, 2) fully coincide with the present data.

Tables 5 and 6 collect the electron delocalization data and NICS values for these compounds. The *cyclo*-$[Be_3]^{2-}$ and *cyclo*-$[Ca_3]^{2-}$ clusters present common features to the *cyclo*-$[Mg_3]^{2-}$ species. As said before, when the *cyclo*-$[M_3]^{2-}$ clusters are complexed with alkali metals, the effect in the 2c- and 3c-DIs depends on two factors that counteract, namely, the reduction of the M–M distances and the charge transfer from the *cyclo*-$[M_3]^{2-}$ clusters to the alkali metals. As can be seen in Tables 1 and 4–6, in general, the second factor is the most important and complexation decreases the 2c- and 3c-ESIs with the exceptions of the 3c-ESI of X_2Be_3 species. For the latter, the reduction of the M–M distances due to complexation becomes a more important factor in determining the 3c-ESIs than the charge transfer.

In general, all the clusters with either one or two metal cations exhibit profiles with large negative NICS values, whereas isolated *cyclo*-$[M_3]^{2-}$ species show a low constant NICS profile (Fig. 4), except for the *cyclo*-$[Be_3]^{2-}$ species. In this latter case, the large negative NICS(0) and NICS(1) values have large in-plane components (the zz-component is significantly smaller) due to the small size of the ring. Inspecting Tables 1 and 4–6, in general (again with the exception of M = Be), we find an increase of aromaticity when going from *cyclo*-$[M_3]^{2-}$ species to $X_n[M_3]^{n-2}$ systems according to NICS predictions while the 3c-ESI predicts a reduction of aromaticity. Thus, there is a clear discrepancy between NICS and 3c-ESI aromaticity predictions in these compounds. This result is not totally unexpected since there are many examples in the literature showing discrepancies in aromaticity trends given by descriptors based on different

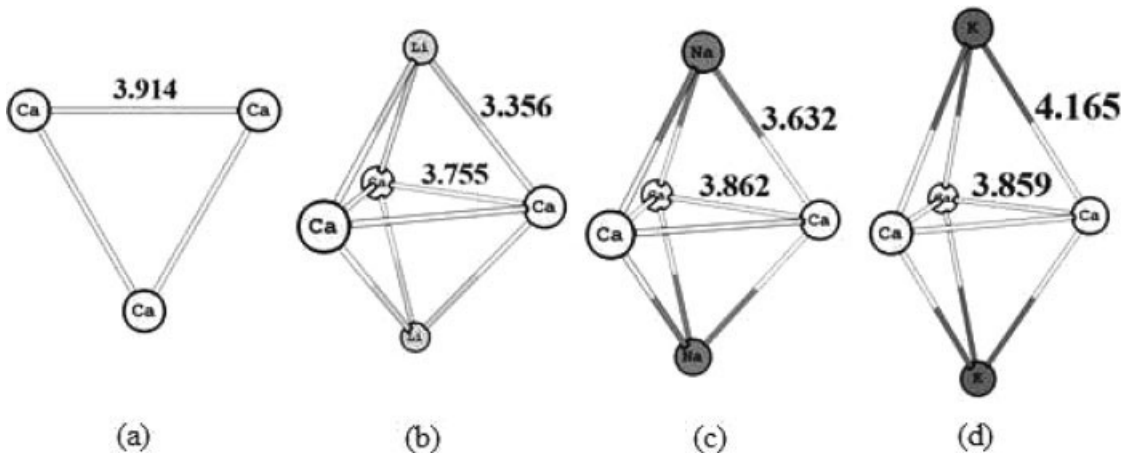

Figure 6. B3LYP/6-311+G(d) optimized structures of calcium species for (a) trigonal planar *cyclo*-$[Ca_3]^{2-}$ (D_{3h}, $^1A_1'$), (b) bipyramidal Li_2Ca_3 (D_{3h}, $^1A_1'$), (c) bipyramidal Na_2Ca_3 (D_{3h}, $^1A_1'$), and (d) bipyramidal K_2Ca_3 (D_{3h}, $^1A_1'$). Bond lengths are given in Å.

Table 5. Total and π Two-Center (2c), Be—Be, and Three-Center (3c), Be—Be—Be, Electron Sharing Indices (ESI, in Electrons), and NICS (in ppm) Indices for *cyclo*-$[Be_3]^{2-}$ (D_{3h}, $^1A_1'$) and X_2Be_3 (D_{3h}, $^1A_1'$), X = Li, Na, K Closed-Shell Species Calculated at B3LYP/6-311+G(d) Level of Theory.

Index	Be_3^{2-}	Li_2Be_3	Na_2Be_3	K_2Be_3
2c-ESI	1.462	1.330	1.229	1.247
2c-ESI π	0.000	0.312	0.238	0.243
3c-ESI	0.471	0.577	0.506	0.517
3c-ESI π	0.000	0.174	0.115	0.118
NICS(0)	−62.88	−42.05	−45.01	−44.14
$NICS(0)_{zz}$	−41.39	−45.31	−46.76	−47.90
NICS(1)	−31.53	−25.28	−28.28	−25.90
$NICS(1)_{zz}$	−33.50	−38.81	−41.25	−42.76

physical properties.[66] Thus, for instance, predictions based on magnetic criteria of aromaticity often deviates from those based on energetic grounds[67] but also in several cases NICS and ESI indices lead to remarkable differences in aromaticity tendencies.[50,68,69] Let us also mention here that while NICS values are computed as a response to an external magnetic field and virtual orbitals are involved in the calculation, in the ESI computation just occupied orbitals are used. This could be the reason for the differences observed.

Many times the apparent contradictions found among differently based indices are overcome by addressing to the so-called multidimensional character of aromaticity.[70] In this way, one can argue that it is understandable that different indices afford divergent orderings since one compound may be more aromatic than other in one dimension and less aromatic in another.[71] The discrepancies sometimes can be solved by using a set of indices based on different physical properties. In this case, the trend given by most of the indices can be taken as the correct one. However, as said before, many useful descriptors that are routinely applied in the classic organic compounds cannot be used in this work. In other cases, one can assess the validity of the indices by applying them to a set of systems having widely accepted aromaticity behaviors.[50] Unfortunately, series of inorganic species showing clear trends in aromaticity are still lacking and, therefore, we cannot used them to discuss whether NICS or 3c-ESI results are the most reliable. Therefore, from our results is not possible to conclude which of the trends (reduction or increase of aromaticity upon alkali metal complexation) is the correct for the *cyclo*-$[M_3]^{2-}$ species. However, it is also true that the two methods agree in that alkali metal complexation leads to important changes in aromaticity and we consider it is worth analyzing both theoretically and experimentally the scope of the aromaticity variations.

Table 6. Total and π Two-Center (2c), Ca—Ca, and Three-Center (3c), Ca—Ca—Ca, Electron Sharing Indices (ESI, in Electrons), and NICS (in ppm) Indices for *cyclo*-$[Ca_3]^{2-}$ (D_{3h}, $^1A_1'$) and X_2Ca_3 (D_{3h}, $^1A_1'$), X = Li, Na, K Closed-Shell Species Calculated at B3LYP/6-311+G(d) Level of Theory.

Index	Ca_3^{2-}	Li_2Ca_3	Na_2Ca_3	K_2Ca_3
2c-ESI	1.705	1.306	1.018	1.096
2c-ESI π	0.000	0.297	0.189	0.206
3c-ESI	0.530	0.351	0.244	0.263
3c-ESI π	0.000	0.109	0.054	0.060
NICS(0)	1.75	−27.07	−25.75	−23.91
$NICS(0)_{zz}$	−10.80	−15.42	−15.02	−15.45
NICS(1)	−0.41	−23.00	−22.73	−20.26
$NICS(1)_{zz}$	−10.65	−19.45	−19.09	−18.45

Aromaticity Tuning

We have shown that the coordination of the alkali metal atoms into the M_3 unit undergoes important changes in its electronic distribution. With this scenario, the next natural question arising is at which extent can the aromaticity of the M_3 ring be

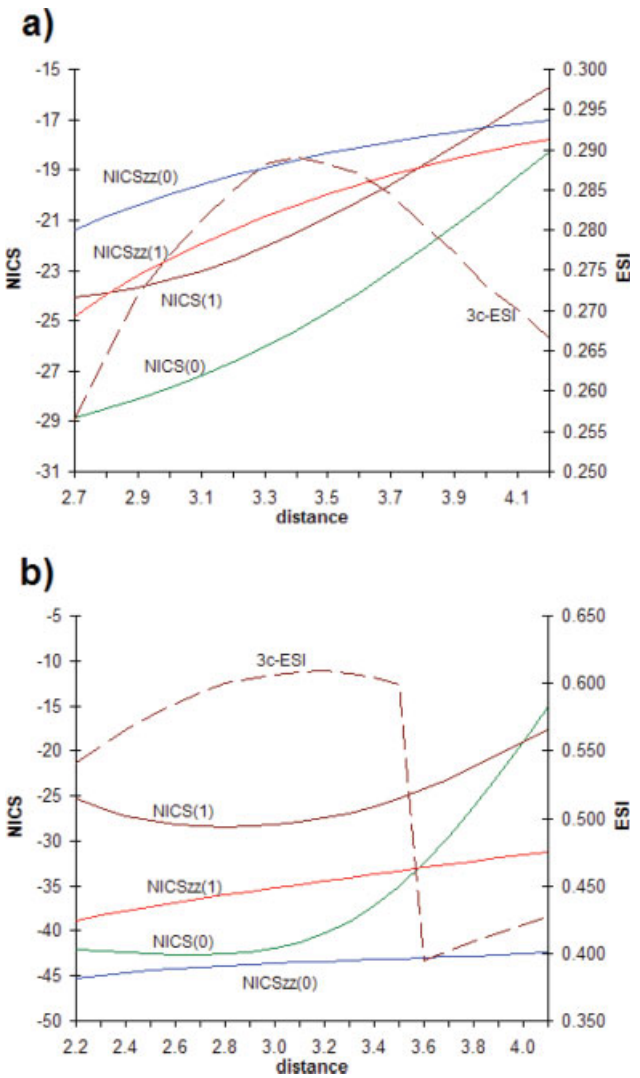

Figure 7. NICS (ppm) and 3c-ESI (electrons) of a) Na_2Mg_3 (D_{3h}) and b) Li_2Be_3 (D_{3h}) as a function of the distance (in Å) between Na or Li and the center of the ring.

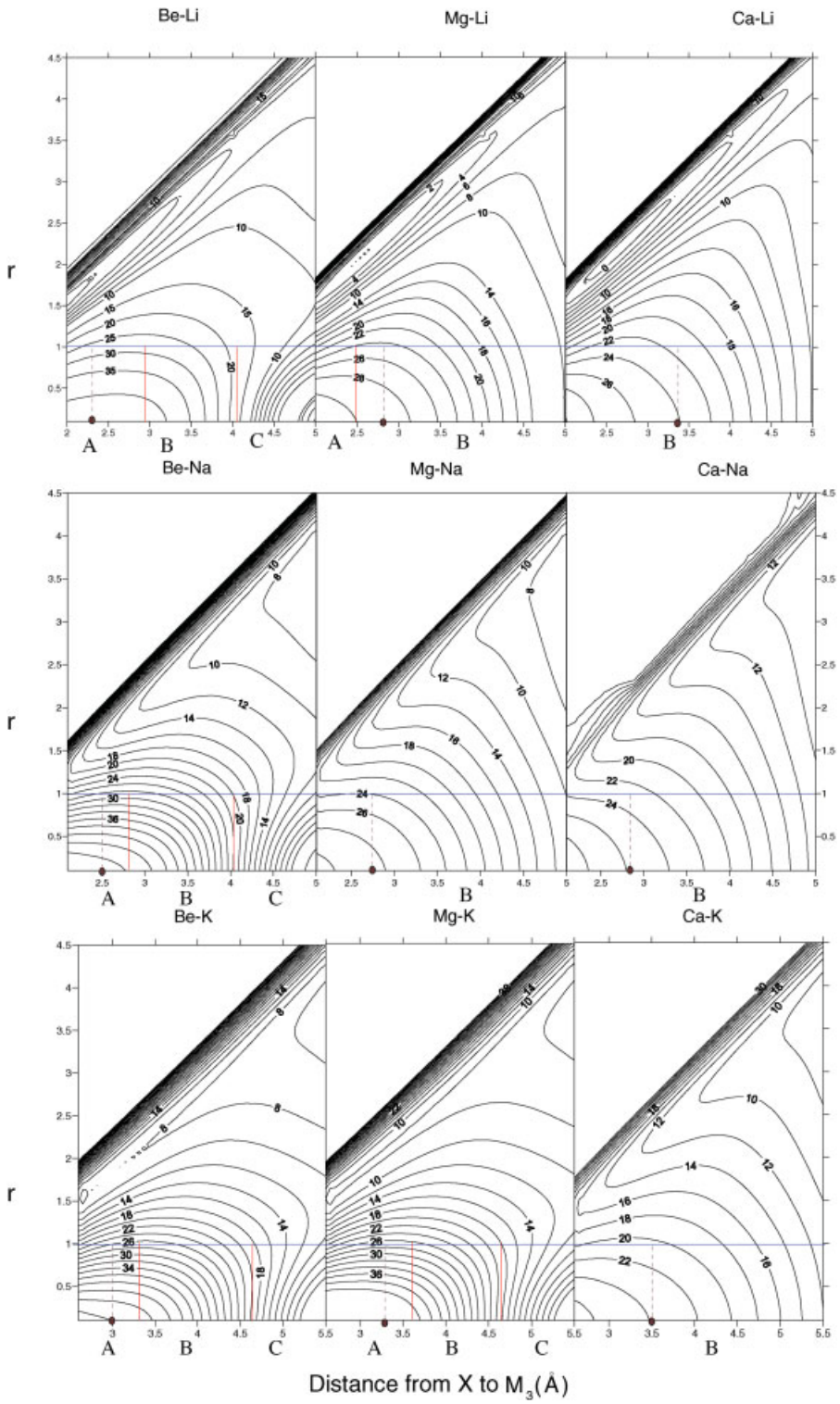

Figure 8. Absolute NICS values at r Å above the M_3 ring, as a function of the distance between X and the center of the M_3 ring (M-X). The horizontal blue line shows the NICS(1) values, while the straight vertical red lines separate the three tuning regions. [Color figure can be viewed in the online issue, which is available at www.interscience.wiley.com.]

influenced by the alkali metal atom distance to the ring? In Figure 7 are analyzed the changes in aromaticity of the M_3 ring for the homolytic dissociation of Na_2Mg_3 bimetallic cluster into 2Na + *cyclo*-[Mg_3] (the ionic dissociation into $2Na^+$ + *cyclo*-$[Mg_3]^{2-}$ is energetically unfavorable in gas-phase) and Li_2Be_3 into 2Li + *cyclo*-[Be_3] species. As it can be seen in Figure 7, the change in the aromaticity of the ring along the reaction coordinate is very important. For the Na_2Mg_3 cluster, there is an increasing monotonic curve in the NICS values when going from Na_2Mg_3 to 2Na + *cyclo*-[Mg_3], thus indicating a continuous reduction of aromaticity as the distance from Na to the center of the *cyclo*-[M_3] ring increases; meanwhile, the 3c-ESI indicates also a decrease in aromaticity when Na cations are going far until 3.4 Å and then it follows the prediction of NICS. In particular, in this zone, the orbital switching occurs and changes the type of aromaticity. This switch does not manifest in NICS calculations but is represented in the 3c-ESI curve. Furthermore, for Li_2Be_3 system, total NICS(0) and NICS(1) scans have a nice agreement with 3c-ESI as it is predicted an augment in aromaticity followed by a continuous decreasing at 3.5 Å, again near to the zone of orbital switching. Unfortunately, because of the lack of proper treatment of static correlation in our calculations, the NICS and 3c-ESI values reported for this region have to be taken with caution. However, we have checked that 3c-ESI scans of some of these clusters performed with the CASSCF(10,10) method yield a similar curve shape as that found with the B3LYP method; so we concluded that the B3LYP results presented here are reliable.

We have calculated NICS profiles at different distances between X (X = Li, Na, and K) and the three possible M_3 units (M = Be, Mg, and Ca). Although the NICS profile is depicted down to 0.5 Å above the X atom (farther values are quite influenced by the X atom), we will focus on the region r = 0–1 Å. By examining the NICS profiles as the distance of X atom to the M_3 unit increases, we can assess the change in aromaticity as a function of the X-M_3 distance. In Figure 8 are depicted the three NICS profiles as the distance of X increases with respect to the three metallic units: Be_3, Mg_3, and Ca_3. In this Figure, one can see the line at r = 1 Å corresponding to NICS(1) values at the different distances of the alkali metal to the center of the M_3 cluster. Perpendicular to this line, there are two straight lines which separate the spectrum in three different regions as follows: *A*, *B*, and *C*. *A* is the region where the NICS profile remains approximately constant, region *B* is where the NICS profiles change, and region *C* begins at the value of X-M_3 distance where the profile becomes flat (straight vertical line). Additionally, there is a dashed line which shows the equilibrium X-M_3 distance. It is worth noting here that variations of NICS with the distance to the M_3 unit are not surprising in the light of the report by Havenith et al.[68] showing that maps of induced current density in $Li_3Al_4^-$ and Li_4Al_4 vary strongly with the distance to the plotting and Al_4 planes.

There are basically two different kinds of NICS profiles with X-M_3 distance. Those that exhibit the three regions *A*, *B*, and *C*, and the rest which have only the *B* region. For the former (Be_3 clusters and K_2Mg_3), the optimal X-M_3 distance lies in the region *A*, thus one expects these clusters show very little dependence of aromaticity with small changes of X-M_3 distance. Only large variations in the coordination distance will lead to substantial aromaticity changes. On the contrary, the rest of the clusters do not have constant NICS profile region, thus leading to sensible changes when X-M_3 distance is modified. The only exception is the Li_2Mg_3 cluster, which exhibits the *A* region, however, the optimal X-M_3 distance lies in the *B* region, providing different NICS profiles for larger Li-Mg_3 distances. This means that not all the clusters studied here are good candidates for observing experimentally a significant change in aromaticity by modifying the M-X distance. This finding may open the way to control reactivity based on aromaticity tuning. We hope this result will stimulate the research of new materials with this kind of reactivity changes.

Conclusions

In this article, we have shown that the all-metal aromatic species do not only have different types of aromaticity (σ-, π-, δ-, or φ-aromaticity) but also that the type of aromaticity of a given species can change depending on external conditions, such as the presence of alkali metals. We have found that the coordination of one or two Na cations within the *cyclo*-$[Mg_3]^{2-}$ unit leads to a switch on the aromaticity behavior of this species. Such change in the type of aromaticity is also found in all $[M_3]^{-2}$ rings (M = Be, Mg, and Ca) when coordinated to alkali metal.

The aromaticity of the trigonal [M_3] rings can be tuned by simply controlling the distance from X to the center of the ring. This is especially true for Na_2Mg_3, Li_2Mg_3, and X_2Ca_3 that can undergo drastic aromaticity alterations by changing the distance from X to the center of the M_3 ring, whereas X_2Be_3 and K_2Mg_3 clusters have been shown to be highly resistant to small perturbations of the distance between X and the M_3 unit. This result may have implications in inorganic chemistry, since control of aromaticity may also help to control reactivity of all-metal aromatic clusters.

Acknowledgments

The authors thank the Centre de Supercomputació de Catalunya (CESCA) for providing partial computer time. The authors are also grateful to the referees who help them to improve the quality of this article. Dr. Pedro Salvador is acknowledged for assistance with the FUZZY program. They are also thankful to Dr. Clémence Corminboeuf for helping us with the use of the NBO 5.0 program.

References

1. (a) Li, X.; Kuznetsov, A. E.; Zhang, H.-F.; Boldyrev, A. I.; Wang, L.-S. Science 2001, 291, 859; (b) Kuznetsov, A. E.; Birch, K. A.; Boldyrev, A. I.; Li, X.; Zhai, H.-J.; Wang, L.-S. Science 2003, 300, 622.
2. Boldyrev, A. I.; Wang, L. S. Chem Rev 2005, 105, 3716.
3. Datta, A.; Mallajosyula, S. S.; Pati, S. K. Acc Chem Res 2007, 40, 213.
4. Tsipis, C. A. Coord Chem Rev 2005, 249, 2740.

5. Zubarev, D. Y.; Averkiev, B. B.; Zhai, H.-J.; Wang, L.-S.; Boldyrev, A. I. Phys Chem Chem Phys 2008, 10, 257.
6. (a) Li, Z.; Zhao, C.; Chen, L. J. Mol Struct (THEOCHEM) 2007, 810, 1; (b) Mercero, J. M.; Formoso, E.; Matxain, J. M.; Eriksson, L. A.; Ugalde, J. M. Chem Eur J 2006, 12, 4495; (c) Mercero, J. M.; Ugalde, J. M. J Am Chem Soc 2004, 126, 3380; (d) Yang, L. M.; Ding, Y. H.; Sun, C. C. Chemphyschem 2006, 7, 2478; (e) Yang, L.-M.; Ding, Y.-H.; Sun, C.-C. Chem Eur J 2007, 13, 2546.
7. Chattaraj, P. K.; Giri, S. J Mol Struct (THEOCHEM) 2008, 865, 53.
8. Kuznetsov, A. E.; Boldyrev, A. I.; Zhai, H. J.; Li, X.; Wang, L. S. J Am Chem Soc 2002, 124, 11791.
9. Datta, A.; Pati, S. K. J Phys Chem A 2004, 108, 9527.
10. (a) Chandrasekhar, J.; Jemmis, E. D.; Schleyer, P. v. R. Tetrahedron Lett 1979, 20, 3707; (b) Schleyer, P. v. R.; Jiao, H.; Glukhovtsev, M. N.; Chandrasekhar, J.; Kraka, E. J Am Chem Soc 1994, 116, 10219.
11. (a) Martín-Santamaría, S.; Rzepa, H. S. Chem Commun 2000, 1503; (b) Präsang, C.; Mlodzianowska, A.; Sahin, Y.; Hofmann, M.; Geiseler, G.; Massa, W.; Berndt, A. Angew Chem Int Ed Engl 2002, 41, 3380; (c) Wodrich, M. D.; Corminboeuf, C.; Park, S. S.; Schleyer, P. v. R. Chem Eur J 2007, 13, 4582.
12. Alexandrova, A. N.; Boldyrev, A. I. J Phys Chem A 2003, 107, 554.
13. (a) Li, Z. H.; Moran, D.; Fan, K. N.; Schleyer, P. v. R. J Phys Chem A 2005, 109, 3711; (b) Minkin, V. I.; Glukhovtsev, M. N.; Simkin, B. Y. J Mol Struct (THEOCHEM) 1988, 181, 93.
14. (a) Huang, X.; Zhai, H. J.; Kiran, B.; Wang, L. S. Angew Chem Int Ed 2005, 44, 7251; (b) Wannere, C. S.; Corminboeuf, C.; Wang, Z. X.; Wodrich, M. D.; King, R. B.; Schleyer, P. v. R. J Am Chem Soc 2005, 127, 5701; (c) Zhai, H.-J.; Averkiev, B. B.; Zubarev, D. Y.; Wang, L.-S.; Boldyrev, A. I. Angew Chem Int Ed 2007, 46, 4277.
15. Tsipis, A. C.; Kefalidis, C. E.; Tsipis, C. A. J Am Chem Soc 2008, 130, 9144.
16. Zhan, C.-G.; Zheng, F.; Dixon, D. A. J Am Chem Soc 2002, 124, 14795.
17. Havenith, R. W. A.; De Proft, F.; Fowler, P. W.; Geerlings, P. Chem Phys Lett 2005, 407, 391.
18. Jiao, H.; Schleyer, P. v. R.; Glukhoutsev, M. N. J Phys Chem 1996, 100, 12299.
19. (a) Dewar, M. J. S. J Am Chem Soc 1984, 106, 669; (b) Cremer, D.; Gauss, J. J Am Chem Soc 1986, 108, 7467; (c) Cremer, D. Tetrahedron 1988, 44, 7427.
20. (a) Furusaki, A. J Mol Struct (THEOCHEM) 1996, 362, 365; (b) Goller, A.; Clark, T. J Mol Model 2000, 6, 133; (c) Ichinohe, M.; Igarashi, M.; Sanuki, K.; Sekiguehi, A. J Am Chem Soc 2005, 127, 9978; (d) King, R. B. Inorg Chim Acta 2003, 350, 126; (e) Lee, V. Y.; Sekiguchi, A. Angew Chem Int Ed 2007, 46, 6596.
21. Hofmann, M.; Berndt, A. Heteroat Chem 2006, 17, 224.
22. Kuznetsov, A. E.; Boldyrev, A. I. Chem Phys Lett 2004, 388, 452.
23. Jiménez-Halla, J. O. C.; Matito, E.; Robles, J.; Solà, M. J Organomet Chem 2006, 691, 4359.
24. Roy, D. R.; Chattaraj, P. K. J Phys Chem A 2008, 112, 1612.
25. Schleyer, P. v. R.; Maerker, C.; Dransfeld, A.; Jiao, H.; van Eikema Hommes, N. J. R. J Am Chem Soc 1996, 118, 6317.
26. Chen, Z.; Wannere, C. S.; Corminboeuf, C.; Puchta, R.; Schleyer, P. v. R. Chem Rev 2005, 105, 3842.
27. Schleyer, P. v. R.; Jiao, H. J.; van Eikema Hommes, N. J. R.; Malkin, V. G.; Malkina, O. L. J Am Chem Soc 1997, 119, 12669.
28. (a) Becke, A. D. J Chem Phys 1993, 98, 5648; (b) Lee, C.; Yang, W.; Parr, R. G. Phys Rev B 1988, 37, 785.
29. (a) Krishnan, R.; Binkley, J. S.; Seeger, R.; Pople, J. A. J. Chem Phys 1980, 72, 650; (b) Frisch, M. J.; Pople, J. A.; Binkley, J. S. J Chem Phys 1984, 80, 3265.
30. Frisch, M. J.; Trucks, G. W.; Schlegel, H. B.; Scuseria, G. E.; Robb, M. A.; Cheeseman, J. R.; Montgomery, J. A., Jr.; Vreven, T.; Kudin, K. N.; Burant, J. C.; Millam, J. M.; Iyengar, S. S.; Tomasi, J.; Barone, V.; Mennucci, B.; Cossi, M.; Scalmani, G.; Rega, N.; Petersson, G. A.; Nakatsuji, H.; Hada, M.; Ehara, M.; Toyota, K.; Fukuda, R.; Hasegawa, J.; Ishida, M.; Nakajima, T.; Honda, Y.; Kitao, O.; Nakai, H.; Klene, M.; Li, X.; Knox, J. E.; Hratchian, H. P.; Cross, J. B.; Adamo, C.; Jaramillo, J.; Gomperts, R.; Stratmann, R. E.; Yazyev, O.; Austin, A. J.; Cammi, R.; Pomelli, C.; Ochterski, J.; Ayala, P. Y.; Morokuma, K.; Voth, G. A.; Salvador, P.; Dannenberg, J. J.; Zakrzewski, V. G.; Dapprich, S.; Daniels, A. D.; Strain, M. C.; Farkas, O.; Malick, D. K.; Rabuck, A. D.; Raghavachari, K.; Foresman, J. B.; Ortiz, J. V.; Cui, Q.; Baboul, A. G.; Clifford, S.; Cioslowski, J.; Stefanov, B. B.; Liu, G.; Liashenko, A.; Piskorz, P.; Komaromi, I.; Martin, R. L.; Fox, D. J.; Keith, T.; Al-Laham, M.; Peng, C.; Nanayakkara, A.; Challacombe, M.; Gill, P. M. W.; Johnson, B. G.; Chen, W.; Wong, M. W.; González, C.; Pople, J. A. Gaussian 03 Package; Pittsburgh, PA, 2003.
31. (a) Fradera, X.; Austen, M. A.; Bader, R. F. W. J Phys Chem A 1999, 103, 304; (b) Fradera, X.; Poater, J.; Simon, S.; Duran, M.; Solà, M. Theor Chem Acc 2002, 108, 214.
32. (a) Giambiagi, M.; de Giambiagi, M. S.; Mundim, K. C. Struct Chem 1990, 1, 423; (b) Bochicchio, R.; Ponec, R.; Torre, A.; Lain, L. Theor Chem Acc 2001, 105, 292.
33. Ponec, R.; Mayer, I. J Phys Chem A 1997, 101, 1738.
34. Matito, E. ESI-3D Program; IQC: Girona, 2006. Available at: http://iqc.udg.es/∼eduard/ESI.
35. (a) Ponec, R.; Cooper, D. L. Int J Quantum Chem 2004, 97, 1002; (b) Ponec, R.; Yuzhakov, G.; Tantillo, D. J. J Org Chem 2004, 69, 2992.
36. Bultinck, P.; Ponec, R.; Van Damme, S. J Phys Org Chem 2005, 18, 706.
37. Mayer, I.; Salvador, P. Chem Phys Lett 2004, 383, 368.
38. Matito, E.; Solà, M.; Salvador, P.; Duran, M. Faraday Discuss 2007, 135, 325.
39. Poater, J.; Solà, M.; Duran, M.; Fradera, X. Theor Chem Acc 2002, 107, 362.
40. Mayer, I.; Salvador, P. Program FUZZY; IQC: Girona, 2003. Available at: http://occam.chemres.hu/programs.
41. (a) Stanger, A. J Org Chem 2006, 71, 883; (b) Stanger, A. Chem Eur J 2006, 12, 2745.
42. Tsipis, C. A.; Depastas, I. G.; Kefalidis, C. E. J Comput Chem 2007, 28, 1893.
43. Poater, J.; Duran, M.; Solà, M.; Silvi, B. Chem Rev 2005, 105, 3911.
44. Poater, J.; Fradera, X.; Duran, M.; Solà, M. Chem Eur J 2003, 9, 400.
45. Matito, E.; Duran, M.; Solà, M. J Chem Phys 2005, 122, 014109; erratum, íbid 2006, 125, 059901.
46. Kruszewski, J.; Krygowski, T. M. Tetrahedron Lett 1972, 13, 3839.
47. (a) Cyrański, M. K. Chem Rev 2005, 105, 3773; (b) Hehre, W. J.; McIver, R. T.; Pople, J. A.; Schleyer, P. v. R. J Am Chem Soc 1974, 96, 7162.
48. Wodrich, M. D.; Wannere, C. S.; Mo, Y.; Jarowski, P. D.; Houk, K. N.; Schleyer, P. v. R. Chem Eur J 2007, 13, 7731.
49. (a) Giambiagi, M.; de Giambiagi, M. S.; dos Santos, C. D.; de Figueiredo, A. P. Phys Chem Chem Phys 2000, 2, 3381; (b) Bultinck, P.; Fias, S.; Ponec, R. Chem Eur J 2006, 12, 8813; (c) Mandado, M.; González-Moa, M. J.; Mosquera, R. A. J Comput Chem 2007, 28, 127.
50. Feixas, F.; Matito, E.; Poater, J.; Solà, M. J Comput Chem 2008, 29, 1543.
51. (a) Grimme, S. J Am Chem Soc 1992, 114, 10542; (b) Rice, J. E.; Lee, T. J.; Remington, R. B.; Allen, W. D.; Clabo, D. A., Jr.; Schaefer, H. F., III. J Am Chem Soc 1987, 109, 2902.

52. Schleyer, P. v. R.; Manoharan, M.; Wang, Z. X.; Kiran, B.; Jiao, H. J.; Puchta, R.; van Eikema Hommes, N. J. R. Org Lett 2001, 3, 2465.
53. (a) Reed, A. E.; Curtiss, L. A.; Weinhold, F. Chem Rev 1988, 88, 899; (b) Glendening, E. D.; Badenhoop, J. K.; Reed, A. E.; Carpenter, J. E.; Bohmann, J. A.; Morales, C. M.; Weinhold, F.; NBO 5.0 Program; Theoretical Chemistry Institute, University of Wisconsin: Madison, 2001.
54. (a) Becke, A. D.; Edgecombe, K. E. J. Chem Phys 1990, 92, 5397; (b) Matito, E.; Silvi, B.; Duran, M.; Solà, M. J Chem Phys 2006, 125, 024301; (c) Silvi, B.; Savin, A. Nature 1994, 371, 683.
55. Savin, A.; Nesper, R.; Wengert, S.; Fassler, T. F. Angew Chem Int Ed Engl 1997, 36, 1809.
56. Matito, E.; Poater, J.; Duran, M.; Solà, M. Chemphyschem 2006, 7, 111.
57. Santos, J. C.; Andrés, J.; Aizman, A.; Fuentealba, P. J Chem Theor Comput 2005, 1, 83.
58. (a) Noury, S.; Krokidis, X.; Fuster, F.; Silvi, B. Topmod Package, Université Pierre et Marie Curie, Paris, 1997. Available at: http://www.lct.jussie.fr/pageperaso/silvi/topmod-english.html;(b) Noury, S.; Krokidis, X.; Fuster, F.; Silvi, B. Comput Chem 1999, 23, 597.
59. Thomas, O. C.; Zheng, W.; Xu, S.; Bowen, K. H, Jr. Phys Rev Lett 2002, 89, 213401.
60. Lambrecht, D. S.; Fleig, T.; Sommerfeld, T. J Phys Chem A 2008, 112, 2855.
61. Zubarev, D. Y.; Boldyrev, A. I. J Phys Chem A 2008, 112, 7984.
62. Lambrecht, D. S.; Fleig, T. J Phys Chem A 2008, 112, 7986.
63. Güell, M.; Matito, E.; Luis, J. M.; Poater, J.; Solà, M. J Phys Chem A 2006, 110, 11569.
64. Kaplan, I. G.; Roszak, S.; Leszczynski, J. J Chem Phys 2000, 113, 6245.
65. Feixas, F.; Jiménez-Halla, J. O. C.; Matito, E.; Poater, J.; Solà, M. Pol J Chem 2007, 81, 783.
66. Poater, J.; García-Cruz, I.; Illas, F.; Solà, M. Phys Chem Chem Phys 2004, 6, 314.
67. Aihara, J. J Am Chem Soc 2006, 128, 2873.
68. Havenith, R. W. A.; Fowler, P. W.; Steiner, E.; Shetty, S.; Kanhere, D.; Pal, S. Phys Chem Chem Phys 2004, 6, 285.
69. (a) Khatua, S.; Roy, D. R.; Bultinck, P.; Bhattacharjee, M.; Chattaraj, P. K. Phys Chem Chem Phys 2008, 6, 285; (b) Roy, D. R.; Bultinck, P.; Subramanian, V.; Chattaraj, P. K. J Mol Struct (THEOCHEM) 2008, 854, 35.
70. (a) Katritzky, A. R.; Barczynski, P.; Musumarra, G.; Pisano, D.; Szafran, M. J Am Chem Soc 1989, 111, 7; (b) Katritzky, A. R.; Jug, K.; Oniciu, D. C. Chem Rev 2001, 101, 1421; (c) Katritzky, A. R.; Karelson, M.; Sild, S.; Krygowski, T. M.; Jug, K. J Org Chem 1998, 63, 5228; (d) Krygowski, T. M.; Cyrański, M. K. Chem Rev 2001, 101, 1385; (e) Cyrański, M. K.; Krygowski, T. M.; Katritzky, A. R.; Schleyer, P. v. R. J Org Chem 2002, 67, 1333.
71. Krygowski, T. M.; Cyrański, M. K.; Czarnocki, Z.; Häfelinger, G.; Katritzky, A. R. Tetrahedron 2000, 56, 1783.